

Effects and uptake of gold nanoparticles deposited at the air–liquid interface of a human epithelial airway model

C. Brandenberger^{a,*}, B. Rothen-Rutishauser^a, C. Mühlfeld^b, O. Schmid^c, G.A. Ferron^c, K.L. Maier^c, P. Gehr^a, A.-G. Lenz^c

^a Institute of Anatomy, Division of Histology, University of Bern, Bern, Switzerland

^b Institute of Anatomy and Cell Biology, Justus-Liebig-University Giessen, Giessen, Germany

^c Institute of Lung Biology and Disease, Helmholtz Zentrum München, Neuherberg, Germany

ARTICLE INFO

Article history:

Received 13 July 2009

Revised 9 September 2009

Accepted 22 September 2009

Available online 29 September 2009

Keywords:

Gold nanoparticles

Nanotoxicology

Human epithelial airway model

Air–liquid exposure

Particle lung interaction

ABSTRACT

The impact of nanoparticles (NPs) in medicine and biology has increased rapidly in recent years. Gold NPs have advantageous properties such as chemical stability, high electron density and affinity to biomolecules, making them very promising candidates as drug carriers and diagnostic tools. However, diverse studies on the toxicity of gold NPs have reported contradictory results. To address this issue, a triple cell co-culture model simulating the alveolar lung epithelium was used and exposed at the air–liquid interface.

The cell cultures were exposed to characterized aerosols with 15 nm gold particles (61 ng Au/cm² and 561 ng Au/cm² deposition) and incubated for 4 h and 24 h. Experiments were repeated six times. The mRNA induction of pro-inflammatory (TNF α , IL-8, iNOS) and oxidative stress markers (HO-1, SOD2) was measured, as well as protein induction of pro- and anti-inflammatory cytokines (IL-1, IL-2, IL-4, IL-6, IL-8, IL-10, GM-CSF, TNF α , INF γ). A pre-stimulation with lipopolysaccharide (LPS) was performed to further study the effects of particles under inflammatory conditions. Particle deposition and particle uptake by cells were analyzed by transmission electron microscopy and design-based stereology.

A homogeneous deposition was revealed, and particles were found to enter all cell types. No mRNA induction due to particles was observed for all markers. The cell culture system was sensitive to LPS but gold particles did not cause any synergistic or suppressive effects.

With this experimental setup, reflecting the physiological conditions more precisely, no adverse effects from gold NPs were observed. However, chronic studies under *in vivo* conditions are needed to entirely exclude adverse effects.

© 2009 Elsevier Inc. All rights reserved.

Introduction

During the last years the impact of nanoparticles (NPs) in medicine and biology has increased rapidly, especially for bioimaging (Jain et al., 2008), biosensing (Olofsson et al., 2003) and drug delivery (Dhar et al., 2008; Joshi et al., 2006). Gold NPs are chemically stable, electron

dense and possess an affinity to biomolecules, such as amino acids (Selvakannan et al., 2004), proteins (Wangoo et al., 2008) and DNA (Rosi et al., 2006), making them suitable as drug carriers and imaging reagents. Promising results have been obtained in cancer research where conjugated gold NPs have been used for cancer detection and treatment *in vitro* (Chen et al., 2007; Khaing Oo et al., 2008; Li et al., 2009).

Despite the potential medical benefits of gold NPs, it remains unclear whether their use in biological organisms and humans, in particular, will be safe. A variety of toxicity tests *in vitro* were reported for gold NPs providing controversial results. Most studies have excluded the toxicity of gold NPs (4 nm–18 nm in diameter) (Connor et al., 2005; Khan et al., 2007; Shukla et al., 2005), studying cell viability, pro-apoptotic effects, oxidative stress and inflammatory response. In contrast, cytotoxic and pro-apoptotic effects of gold particles ≤ 2 nm were reported (Pan et al., 2007; Tsoli et al., 2005), as well as the impact of the charge of surface coatings on 2 nm particles on the reduction of cell viability (Goodman et al., 2004). Furthermore, exposure of fibroblasts to 13 nm gold particles caused morphological

Abbreviations: ALICE, air–liquid interface cell exposure system; ANOVA, analysis of variance; cDNA, complementary deoxyribonucleic acid; EC, epithelial cells; GM-CSF, granulocyte macrophage colony stimulating factor; HO-1, hemoxygenase 1; IC₅₀, concentration causing 50% inhibition; IL-1 β , interleukin-1 β ; IL-2, interleukin-2; IL-4, interleukin-4; IL-6, interleukin-6; IL-8, interleukin-8; IL-10, interleukin-10; INF γ , interferon γ ; iNOS, inducible nitric oxide synthase; LC₅₀, concentration causing 50% lethality; LPS, lipopolysaccharide; LSM, laser scanning microscopy; MDCC, monocyte derived dendritic cells; MDM, monocyte derived macrophages; mRNA, messenger ribonucleic acid; NPs, nanoparticles; NO, nitric oxide; PBS, phosphate buffered saline; PCR, polymerase chain reaction; RCF, relative centrifugal force; SOD2, super oxide dismutase 2; TEM, transmission electron microscopy; TNF α , tumor necrosis factor α .

* Corresponding author. University of Bern, Institute of Anatomy, Baltzerstrasse 2, CH-3000 Bern 9, Switzerland. Fax: +41 31 6313807.

E-mail address: brandenberger@ana.unibe.ch (C. Brandenberger).

changes in the cytoskeleton and a reduction in cell proliferation (Pernodet et al., 2006). A pro-inflammatory response was found after exposure to bovine serum albumin coated 25 nm gold particles in an epithelial airway model (Rothen-Rutishauser et al., 2007).

The reasons for these controversial results might include different experimental set ups and particle characteristics. Recent studies have identified that a number of important parameters influence the toxicity of NPs (Nel et al., 2006; Oberdörster et al., 2005), such as dose (Kwon et al., 2009), size (Kreyling et al., 2006), shape (Oberdörster et al., 2005), bulk material (Hussain et al., 2005), surface charge (Cho et al., 2009; Goodman et al., 2004), surface area (Brandenberger et al., 2009; Stoeger et al., 2006), as well as the composition of the exposure medium (Herzog et al., 2009b).

All the studies on gold NPs, discussed previously, were performed in cell cultures under submerged conditions with the particles suspended in different media. Besides the effects of the media on agglomeration status, the movements of single NPs in fluids are mainly driven by diffusion and not by sedimentation (Limbach et al., 2005; Teeguarden et al., 2007). As a consequence from the latter the probability of agglomerates to settle down onto the cell culture is higher than that for single NPs, thus increasing the possibility of attributing the observations to the wrong kind of particles (Limbach et al., 2005). A direct deposition of the particles on the cells at the air-liquid interface has the advantage of minimizing these effects, resulting in a more reliable dosimetry and less particle agglomeration. The air-liquid interface exposure scenario not only shows ideal characteristics to study particle-cell interactions but also mimics particle deposition in the respiratory tract after inhalation and it is conceivable that the cellular response to particle exposure is different for submerged and air-liquid interface culture conditions.

Lung epithelial cells represent, along with alveolar macrophages, the first line of cellular defense against inhaled particles. These cells participate in the initiation and modulation of the inflammatory response by the production of chemokines. Of particular interest is the involvement of dendritic cells, which are present at the base of the epithelium and are the most competent antigen presenting cells in the lung (Holt et al., 1990). Therefore, in this study an *in vitro* co-culture model of the human epithelial airway barrier was used (Blank et al., 2007; Rothen-Rutishauser et al., 2005), consisting of human blood monocyte derived macrophages and dendritic cells as well as the widely used A549 human alveolar epithelial cell line.

The present study aimed to analyze the inflammatory and oxidative potential of 15 nm gold NPs in the triple cell co-culture model exposed at the air-liquid interface with a newly developed exposure system (Schmid et al., 2009), which allows for efficient, spatially uniform and dose-controlled exposure of cells to NPs. In addition, it was investigated whether the gold NPs aggravate or suppress the response to a pro-inflammatory stimulus, a finding previously observed by others (Chan et al., 2006; de Haar et al., 2006; Herzog et al., 2009a; Hofer et al., 2004).

Materials and methods

Air-liquid interface exposure system

The cell cultures were exposed to the particles at the air-liquid interface with an exposure system (ALICE), described by Schmid et al. (2009). Briefly, the ALICE consists of three main components, a *droplet generator* (nebulizer), an *exposure chamber* and a *flow system with an incubation chamber*, which provides temperature and humidity conditions suitable for cell cultivation (temperature: 37 °C; humidity: nearly saturated). A dense cloud of micron-sized droplets (mass median diameter 4.4–5.4 µm; geometric standard deviation: 1.50–1.65 µm) containing the gold NPs was generated by nebulisation of 1 mL NP suspension using a vibrating membrane droplet generator (investigational eFlow, PARI Pharma GmbH, Munich, Germany). This

type of droplet generator (TouchSpray™ technology) utilizes a perforated, piezoelectrically driven vibrating membrane to induce acoustic pressure waves, which periodically press small amounts of liquid through the tapered holes of a membrane. The resulting dense cloud of droplets containing the NPs was transported at a flow rate of 5 L/min into the exposure chamber (20×20×30 cm), where the cultured cells in standard transwell plates were introduced. The nebulizer gradually filled the chamber with the droplet cloud and as soon as the nebulizer was empty, the air flow was stopped and the droplets settled to the ground onto the cells. The deposition occurred due to an effect known as *cloud settling*: the highly concentrated cloud of droplets (80–130 g/m³) gravitated swiftly within 2 s to the bottom of the exposure chamber (400 cm²), was further diverted to all sides by the ground plate of the chamber and formed an almost symmetric pattern of vortices providing gentle but sufficient mixing to establish a spatially uniform cloud layer near the bottom of the chamber.

The ALICE allowed for uniform and efficient deposition (57 ± 7% of the suspension reached the bottom plate of the exposure chamber) of colloidal gold NPs onto the cells at the air-liquid interface. After the exposure procedure, which lasted for about 20 min, the cells were kept under air-liquid interface conditions for post-exposure incubation times of 4 h and 24 h in the cell incubator. The effective dose of gold NPs deposited on the cells in ng/cm² was measured by gamma spectroscopy as described below.

Particles

Commercially available aqueous 15 nm colloidal gold particles from British Biocell International (EM.GC15, Batch 7894, Plano GmbH, Wetzlar, Germany) in a citrate buffer were used. The particle suspension had a nominal concentration of 0.004% gold colloids, corresponding to a mass concentration of 40 µg/mL. A 10-fold concentration of the colloidal gold was achieved by centrifugation of the suspension at 19 RCF (relative centrifugal force) for 20 min and removing 90% of the supernatant without particles. The size of the particles was analysed in suspension by dynamic light scattering (HPPS 5001, Malvern Instruments Ltd, Worcestershire, UK) and post-air-liquid interface exposure by transmission electron microscopy (TEM; Philips CM12, FEI Co. Philips Electron Optics, Zürich, Switzerland; magnification 15,000×) after placing a TEM grid onto the ground plate of the ALICE during some of the experiments. The Au mass deposited on the cells was determined by placing aluminium foil sheets with a size of 8×4 cm on the bottom of the exposure chamber during an exposure run. After neutron activation of Au-197 into Au-198 for 1 h (the neutron flux was about 6×10¹² cm⁻²s⁻¹) the Au mass on the aluminium foil was determined from the intensity of the 412 keV gamma line of Au-198 relative to a known standard.

Cell cultures

A549 cell line. A549 cells, a human alveolar epithelial-like cell line representing the alveolar type II phenotype (Lieber et al., 1976), were obtained from the American Tissue Type Culture Collection (LGC Promochem, Molsheim, France). Cells (passage number 5 to 30) were maintained in RPMI 1640 medium (w/25 mM HEPES, Invitrogen GmbH, Karlsruhe, Germany) with 1% L-glutamine (Invitrogen), 1% penicillin/streptomycin (Biochrom, Germany), and 10% foetal calf serum (FBS Superior Biochrom, Germany). Cells were seeded at a density of 10⁶ cells in 2 mL on BD Falcon™ 6-well plate cell-culture transwells (high pore density PET membranes with a growth area of 4.2 cm² and 3.0 µm pores in diameter; Omnilab GmbH, Munich, Germany). Transwells were placed in BD Falcon™ 6-well tissue culture plates with 2 mL medium in the upper and 3 mL in the lower transwell chamber. Cells were grown on transwell membranes under submerged conditions for 7 days to grow to confluence. The medium was changed twice a week.

The triple cell co-culture. A triple cell co-culture system with A549 alveolar epithelial cells (EC), human blood monocyte derived macrophages (MDM) and dendritic cells (MDDC) was used (Rothen-Rutishauser et al., 2005). A blood donation of 200 mL was centrifuged at 1300 g for 20 min to receive a buffy coat which was further processed according to the method described by Sallusto et al. (1995). Isolated blood monocytes were cultured for 7 days in RPMI 1640 medium with 1% L-glutamine, 1% penicillin/streptomycin, and 5% heat-inactivated human serum. The MDDC differentiation was obtained by an addition of 34 ng/mL IL-4 (Sigma Aldrich GmbH, Munich, Germany) and 50 ng/mL GM-CSF (Sigma Aldrich GmbH, Munich, Germany), whereas the MDM did not receive any additional supplements. The setup of the triple cell co-culture was performed as described previously (Rothen-Rutishauser et al., 2005). The cells were transferred from submerged to air–liquid interface conditions, 24 h prior to particle exposure: The cell culture medium from the upper transwell chamber was removed and the cell culture medium in the lower transwell chamber was replaced by 1.8 mL of fresh medium. In a set of experiments, an inflammatory stimulus was applied 2 h prior to the particle exposure by adding 1 ng/mL lipopolysaccharide (LPS) (*Pseudomonas aeruginosa*, Sigma Aldrich GmbH, Munich, Germany) into the medium of the lower transwell chamber.

Real-time PCR

RNA isolation was done with the Qiagen RNeasy Mini Kit (Qiagen GmbH, Hilden, Germany). The cells were removed from the cell culture membrane with a cell scraper and the lysis buffer provided by the supplier of the Qiagen RNeasy Mini Kit. The cell lysate was then centrifuged in shredder columns (QIAshredder, Qiagen GmbH, Hilden, Germany) for 2 min at 16 RCF. The isolation was performed according to the supplier's manual including a step of DNA digestion (Qiagen GmbH, Hilden, Germany). The purified RNA was eluted in 30 μ L pure H₂O and stored at -70°C .

The RNA concentration was measured with the Nano-Drop-Photometer (NanoDrop ND100 PeqLab, Germany). Transcription was performed with a total amount of 0.5 μ g RNA in a volume of 20 μ L reaction mixture. Alignment of random nonamer primer (5 μ M final concentration) and RNA in H₂O was done at 70°C for 5 min, followed by cooling on ice for 5 min. Mastermix (1 \times First Strand Buffer, 10 mM DTT, 8 U/ μ L Superscript II RT, 2 U/ μ L RNase Inhibitor, Invitrogen GmbH, Karlsruhe, Germany and 0.5 mM 4dNTP, Fermentas GmbH, St. Leon-Rot, Germany) was added and the mixture incubated for 1 h at 42°C , followed by Superscript inactivation for 15 min at 70°C . Complementary DNA (cDNA) was diluted to a concentration of 66 ng/ μ L and stored at -20°C .

The reaction mixture for quantitative real-time PCR contained 200 ng cDNA, 0.4 μ M forward and reverse Primer and Absolute blue QPCR SYBR Green ROX Mix (Thermo Scientific, ABgene, UK). Primer sequences are shown in Table 1. The thermo cyclic protocol was: 1 \times (50°C , 2 min; 95°C , 15 min) 40 \times (95°C , 15s; 60°C , 1 min) followed by a dissociation stage of 95°C , 15s; 60°C , 20 s; 95°C 15 s. The thermo cyclic reaction and software analysis was performed with the 7500 Real-Time PCR System (Applied Biosystem, Darmstadt, Germany).

Bioplex cytokine detection

After 24 h exposure, 1 mL medium from the lower transwell chamber was sampled and immediately frozen and stored at -70°C until the assay was performed. The detection of pro- and anti-inflammatory cytokines released into the culture medium was carried out with the Bio-Plex Pro Human Cytokine 8-Plex Panel for the detection of interleukin-2 (IL-2), interleukin-4 (IL-4), interleukin-6 (IL-6), interleukin-8 (IL-8), interleukin-10 (IL-10), granulocyte macrophage colony stimulating factor (GM-CSF), tumor necrosis factor α

Table 1
Sequences of the used primers.

GENE	Primer forward 5'-3'	Primer reverse 5'-3'
GAPDH	CCATGAGAAGTATGACAACAGCC	TGGCAGGTTTTTCTAGACCC
IL-8	ATGACTTCCAAGCTGGCCGTGGTC	TCTCAGCCCTCTCAAAAACITCTC
TNF α	CCAAAGTAGACCTGCCAGAGA	TCTACTCCCAGGTCCTCTTCA
iNOS	GCCCAAGTCTATGTTCAG	TAGTCCTCGACCTGCTCTC
SOD2	CCTGGAACCTCACATCAACG	AACCTGAGCCTTGGACACC
HO-1	AAGATTGCCAGAAAGCCCTGGAC	AACTGTCGCCACCAGAAAGCTGAG

(TNF α) and interferon γ (INF γ) (BioRad, Munich, Germany). The assay for interleukin-1 β (IL-1 β) was added to the panel. For the cytokine determination 50 μ L cell culture supernatant was used and processed according to the supplier's protocol.

Quantification of MDM, MDDC and EC

The triple cell co-cultures were fixed on the cell culture transwell with 3% paraformaldehyde in phosphate buffered saline (PBS) for 15 min at room temperature and then treated with 0.1 M glycine in PBS for 5 min. Before staining, the cells were permeabilized with 0.2% Triton X-100 in PBS for 15 min at room temperature. MDM were marked for 1 h with the primary antibody mouse anti-human CD14 (Clone UCHM-1, C 7673; Sigma) and MDDC with mouse anti-human CD86 (Clone HB15e, 36931A; PharMingen, BD Biosciences). Goat anti-mouse cyanine 5 (AP124S; Chemicon, VWR International AG, Life Sciences) was used as a secondary detection antibody. The cytoskeleton of all cells was stained with phalloidin Alexa 488 1:100 (R-415; Molecular Probes, Invitrogen AG, Basel, Switzerland). Preparations for optical analysis were mounted in PBS:glycerol (2:1) containing 170 mg/mL Mowiol 4-88 (Calbiochem, VWR International AG, Dietikon, Switzerland). The samples were visualized with an inverted Zeiss laser scanning microscope (LSM) 510 Meta (Axiovert 200 M, Lasers: HeNe 633 nm, and Ar 488 nm). Image processing was performed with the 3D multi-channel image processing software IMARIS (Bitplane AG, Zürich, Switzerland). From each experiment 10 random images with a size of 71 $\mu\text{m} \times 71 \mu\text{m}$ were evaluated and the number of EC, MDM and MDDC per mm^2 was counted.

Transmission electron microscopy

Intracellular particles were visualized by conventional transmission electron microscopy (TEM) and quantified with stereological methods. For TEM analysis, the exposed cells on the transwell membrane were fixed with 2.5% glutaraldehyde in 0.03 M potassium phosphate buffer for at least 24 h. Then they were washed with potassium phosphate buffer, post-fixed with 1% osmium tetroxide in sodium cacodylate buffer, washed with maleate buffer, and stained en bloc with 0.5% uranyl acetate in maleate buffer. Afterwards, the cells were dehydrated in ascending ethanol series, and embedded in epon (Mühlfeld et al., 2007). From the embedded cells, ultrathin sections were cut parallel to the vertical axis of the cells, mounted on copper grids and stained with lead citrate and uranyl acetate. The substances used in this protocol are hazardous and have to be handled carefully according to safety guidelines. All procedures were performed in a hood with additional adequate personal protection. Imaging was done with a Morgani TEM (FEI Co Philips Electron Optics, Zürich, Switzerland).

Intracellular particle quantification by design based stereology

Stereology enables the estimation of three-dimensional structural features (number, length, surface area or volume) from two-dimensional sections. All parameters are first determined as densities, i.e. as estimate per unit reference volume, and are then converted to

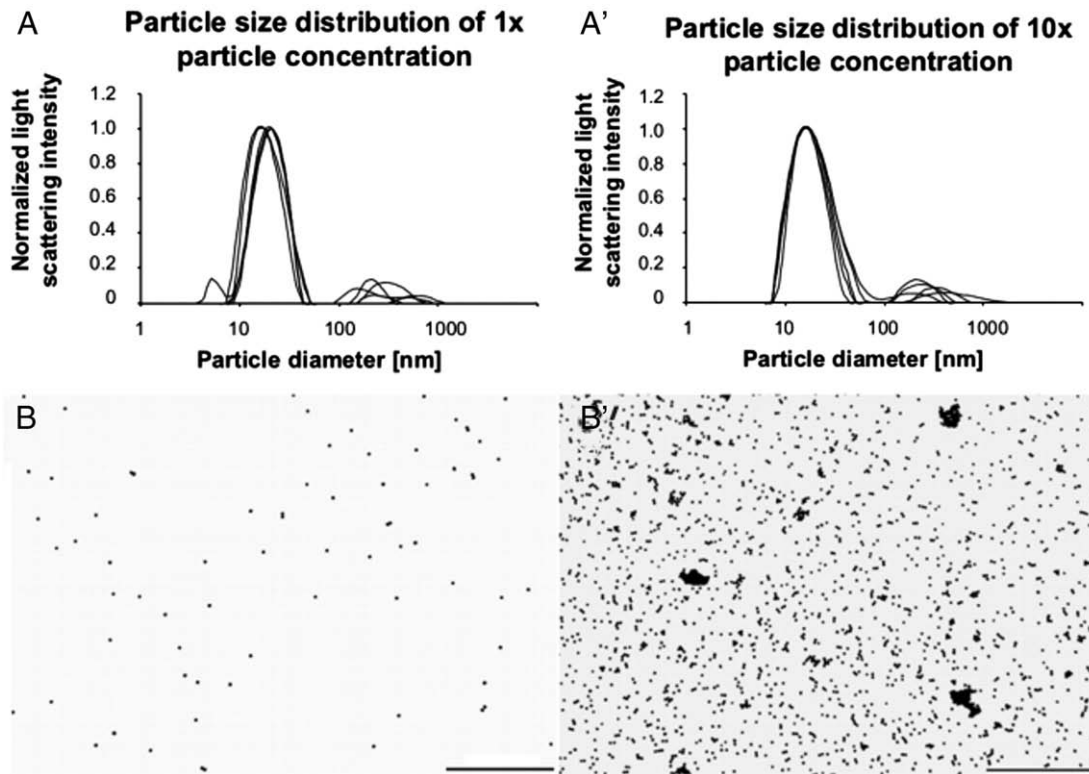


Fig. 1. Particle size distribution of the 15 nm colloidal gold particles prior to exposure (A) and after exposure (B). Size distribution prior to exposure was measured by dynamic light scattering. The pronounced peak near 15 nm indicates that mainly single particles were present for the 1× (A) and the 10× (A') gold concentration. A distribution of the particles after deposition in the ALICE onto TEM grids shows a uniform particle distribution of the 1× (B) and the 10× (B') gold particle deposition (scale bar = 500 nm).

the total value by multiplication with the reference volume. As a reference volume, the cell volume per mm^2 of transwell membrane of the upper and of the basal side of the transwell membrane was estimated. Test fields showing the cells were chosen by systematic uniform random sampling (Mayhew, 2008) at a magnification of 2,200×. A cycloid test line system for surface density estimations on vertical sections (Baddeley et al., 1986) was projected onto each test field with the vertical axis of the test system aligned to the vertical axis of the cells. Intersections (I) of the cycloid test lines with the transwell membrane and the number of test points (P) hitting the cells were counted. The surface density (S_V) of the transwell membrane per unit cell volume was calculated as follows:

$$S_V(\text{Transwell membrane/Cell}) = 2 \times I / (L_T \times P) \quad (1)$$

from the number of intersections (I), number of points (P) and the total length of the test line (L_T) see e.g. Weibel et al. (2007). The amount of particles per cell volume was estimated in random test field areas of ultra thin sections and considering the section thickness as the third volume dimension, as described by Griffiths (1993). Test fields of the cells were taken at a magnification of 22,000× by systematic uniform random sampling and the number of particles per test field were counted within a counting frame. The volume of the test field was calculated from its area (A_T) and the thickness of the ultrathin section (d), which has been estimated by the method of the smallest fold (Small, 1968). The numerical density of particles (N_V) was achieved by:

$$N_V(\text{Nanoparticle/Cell}) = n_p / (n_T \times A_T \times d) \quad (2)$$

from the summed number of particles (n_p) in n test fields (n_T) with the volume $A_T \times d$. The final number of intracellular particles per mm^2 cell culture area (N_A) was then estimated by:

$$N_A(\text{Nanoparticles/Transwell membrane}) = N_V / S_V \quad (3)$$

The intracellular particle number per area was estimated for the upper and for the basal side of the transwell membrane. To achieve the total number of intracellular particles in the co-culture, the numbers at both transwell sides were calculated. The translocation rate from the upper to the basal side of the transwell membrane was determined by comparing the number of intracellular particles at the basal side with the total intracellular number.

Statistics

The statistical analyzes were carried out with the commercial statistical package SigmaSTAT 3.5 (Systat Software Inc., Erkrath, Germany). Due to the small sample sizes ($n = 4-6$), non-parametric tests were used. Kruskal–Wallis One Way Analysis of Variance (ANOVA) on Ranks was performed if more than two groups were compared. Multiple comparisons or multiple comparisons versus negative control were performed with Dunn's method and pairwise comparison with Tukey test. Differences were considered significant at $p < 0.05$. Results are presented as mean \pm standard deviation. Outliers were determined by the Nalimov test at a significance level of $p < 0.05$ and excluded from the studies.

Results

Particle exposure

The particle exposure was performed at the air–liquid interface of the triple cell co-cultures. Using 1 mL of stock solution (40 $\mu\text{g}/\text{mL}$) a deposition of $61 \text{ ng}/\text{cm}^2 \pm 5.5 \text{ ng}/\text{cm}^2$ was obtained, as determined by gamma spectroscopy, and with the 10 fold higher concentration of the stock solution a deposition of $561 \text{ ng}/\text{cm}^2 \pm 48.5 \text{ ng}/\text{cm}^2$ was reached. This corresponds to a deposition efficiency of 61% and 55%, respectively. The quality of the particle suspension prior to the

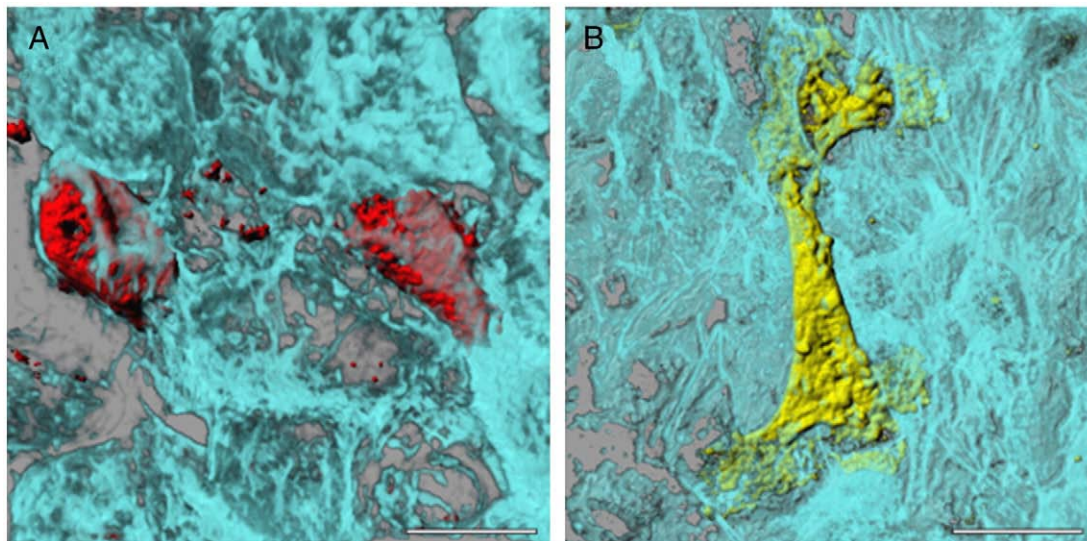


Fig. 2. Laser scanning micrograph of the triple cell co-culture. The macrophages (red) and the epithelial cells (blue) are located at the upper side of the transwell membrane (A, scale bar = 5 μm), whereas the dendritic cells (yellow) are located at the basal side (B, scale bar = 10 μm). An evaluation of the total numbers of cells per mm^2 resulted in 4382 ± 524 epithelial cells, 107 ± 42 macrophages and 81 ± 19 dendritic cells.

exposure was assessed by evaluating the particle size distribution using dynamic light scattering (HPPS 5001, Malvern Instruments Ltd, Worcestershire, UK) (Figs. 1A and A') and the state of agglomeration of the deposited particles was analyzed with TEM by particle exposure onto TEM grids (Figs. 1B and B'). Fig. 1A shows that the suspended gold particles have a dominant mode at 15 nm, which is consistent with single particles or small agglomerates, and a small fraction of larger agglomerates (100 nm–1000 nm). Since the light scattering signal from larger particles is stronger than from smaller particles, Figs. 1A and A' exaggerate the prevalence of larger agglomerates. Similarly, it can be seen from Figs. 1B and B' that the state of agglomeration on the bottom plate of the exposure chamber (location of the cells) is also low. Hence, both analyzes indicate that single particles and small agglomerates were the dominant fraction of those particles reaching the cells.

Quantification of the cells of the triple cell co-culture system

The number of MDM, MDCC and EC was evaluated for each experiment ($n=6$), since the number and quality of primary monocytes may vary and influence the response of the triple cell co-cultures to particles and LPS. Fig. 2A shows the epithelial cells (blue) grown on the upper side of the transwell membrane with MDM on top (red) and Fig. 2B shows a MDCC (yellow) attached to the basal side of the transwell. The cell numbers of all three cell types were 107 ± 42 MDM/ mm^2 , 81 ± 19 MDCC/ mm^2 and 4382 ± 524 EC/ mm^2 . No correlation between high and low response towards LPS and the amount of MDM and MDCC per mm^2 was observed.

Quantitative particle uptake

In order to assess cellular effects upon exposure to particles, it is important to know if the particles can enter the cells or whether they stay attached to the cell membrane. The number of intracellular particles per mm^2 cell culture was evaluated by stereological analysis of TEM micrographs at 4 h and 24 h after exposure, resulting in intracellular numbers of particles per mm^2 of $10.7 \times 10^6 \pm 4.0 \times 10^6$ at 4 h and $11.2 \times 10^6 \pm 7.3 \times 10^6$ at 24 h for the lower and $29.2 \times 10^6 \pm 20.3 \times 10^6$ at 4 h and $35.4 \pm 15.2 \times 10^6$ at 24 h for the higher concentration. As shown in Fig. 3A, the particle uptake was about 60% (57.8% at 4 h and 60.4% at 24 h) of the exposed amount for the lower concentration, whereas only about 20% (17.6% at 4 h and 21.3%

at 24 h) of the exposed particles were taken up at the higher concentration. Comparison between the number of particles at the upper side and at the basal side of the triple cell co-culture shows that

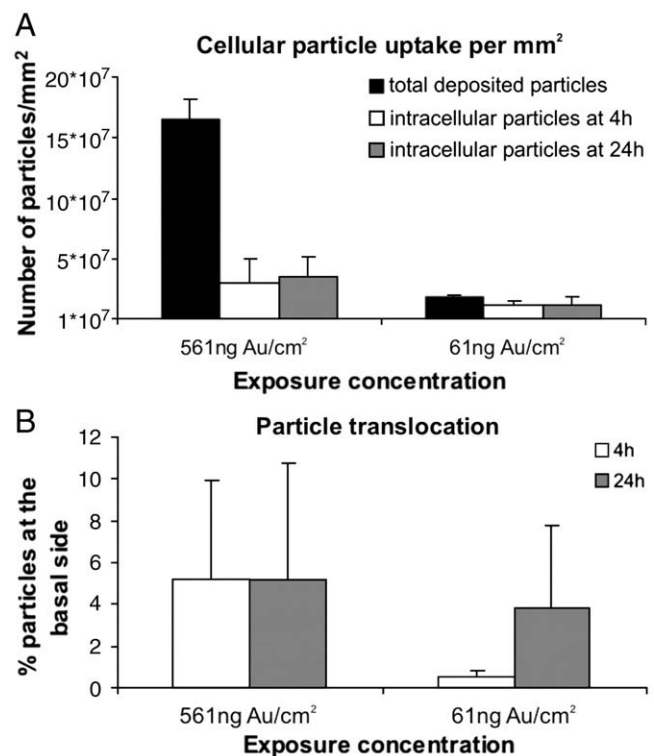


Fig. 3. Particle uptake (A) and translocation (B) in the triple cell co-culture system. The particles have been taken up by the cells and were translocated to the basal side. The particle uptake (A) of both exposure concentrations and incubation times (white and grey bars) has been evaluated by means of design-based stereology and has been compared to the total number of particles deposited (black bar). The degree of uptake was $17.6 \pm 10.7\%$ at 4 h (white bar) and $21.3 \pm 7.3\%$ at 24 h (grey bar) for the high exposure concentration and $57.8 \pm 19.6\%$ at 4 h (white bar) and $60.4 \pm 42.7\%$ at 24 h (grey bar) for the low exposure concentration. The translocation rate (B) from the upper transwell membrane side with epithelial cells and macrophages towards the basal side with dendritic cells is $5.2 \pm 4.8\%$ at 4 h (white bar) and $5.2 \pm 5.6\%$ at 24 h (grey bar) for the high exposure concentration and $0.5 \pm 0.3\%$ at 4 h (white bar) and $3.9 \pm 3.9\%$ at 24 h (grey bar) for the low exposure concentration.

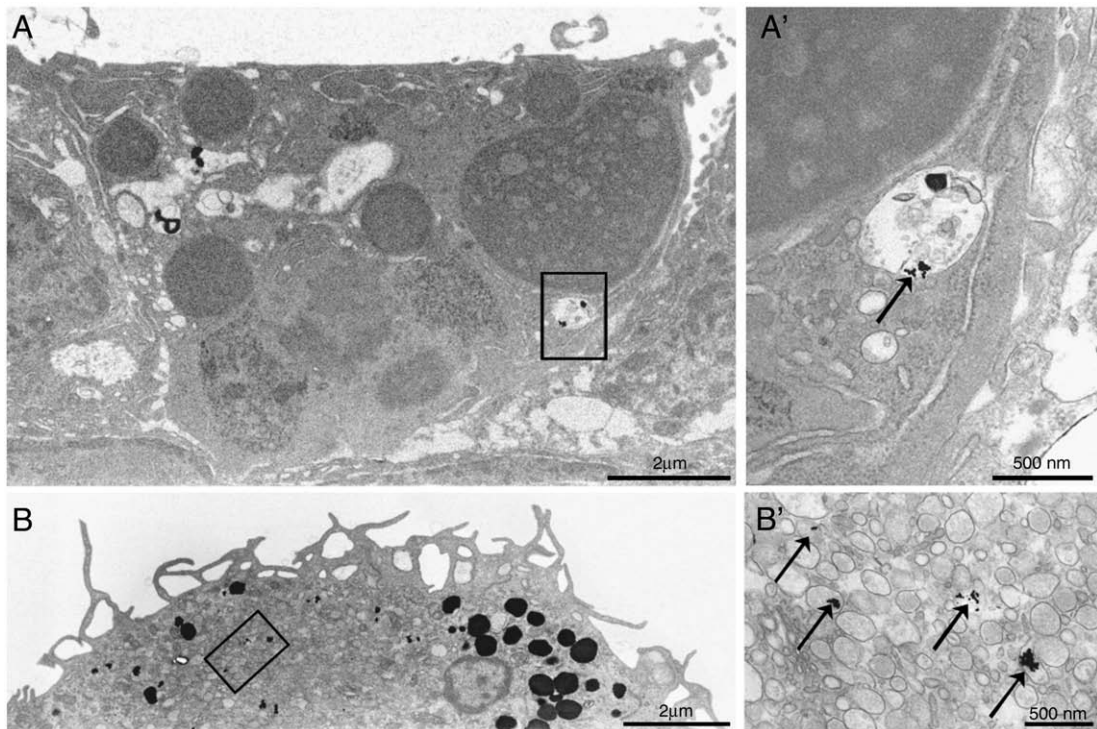


Fig. 4. TEM micrograph of intracellular particles in an epithelial cell (A) at the upper side and dendritic cell (B) at the basal side of the transwell membrane (scale bar = 2 μm). Figures A' and B' show a higher magnification of the black marked box of the left pictures (scale bar = 500 nm). The arrows are pointing towards the particles. The particles were mainly localized in vesicles.

between 0.5% and 5.2% of the particles were translocated from the upper to the basal side and that particle transport occurred at all time points and exposure concentrations (Fig. 3B). However, there was only $0.5 \pm 0.3\%$ translocation rate after 4 h incubation time with the lower particle dose but $3.9 \pm 3.9\%$ after 24 h, although due to high standard deviation no significant difference could be observed, neither for the higher exposure dose ($5.2 \pm 4.8\%$ at 4 h and $5.2 \pm 5.6\%$ at 24 h).

Gold NPs were found in all three cell types; however a quantification of particles per cell type was not possible because of the absence of convenient cell markers at an electron microscopic level. Particles were mostly found in intracellular vesicles as shown in Fig. 4 in an A549 cell (A) and a dendritic cell (B). When counting the number of particles per cell, the largest diameter of single particles and particle agglomerates was also measured. The relative frequency of the agglomerate size at both time points and exposure concentrations is shown in Fig. 5. There was a tendency for more single particles in the cells after exposure to the lower concentration. For both exposure concentrations, an increase of agglomerates, larger than 100 nm in diameter, was observed between 4 h and 24 h.

Cellular responses

The cellular response induced by exposure to the two gold NP concentrations ($1 \times = 61 \text{ ng/cm}^2$ and $10 \times = 561 \text{ ng/cm}^2$ gold particles) was analyzed after post-exposure incubation times of 4 h and 24 h. The pure buffer solution (10 mM aqueous citrate solution) of the particle suspension without the particles was used as a negative control. In some experiments a pre-stimulation with LPS (1 $\mu\text{g/mL}$) was performed 2 h prior to particle exposure to study particle effects under inflammatory conditions. Induction of mRNA (Fig. 6) of three (pro)-inflammatory markers, namely TNF α , IL-8 and inducible nitric oxide synthase (iNOS), as well as of the oxidative stress markers hemeoxygenase-1 (HO-1) and superoxide dismutase 2 (SOD2) were measured. In addition, the protein expression of pro- and anti-inflammatory cytokines, such as IL-1 β , IL-2, IL-4, IL-6, IL-8, IL-10, GM-

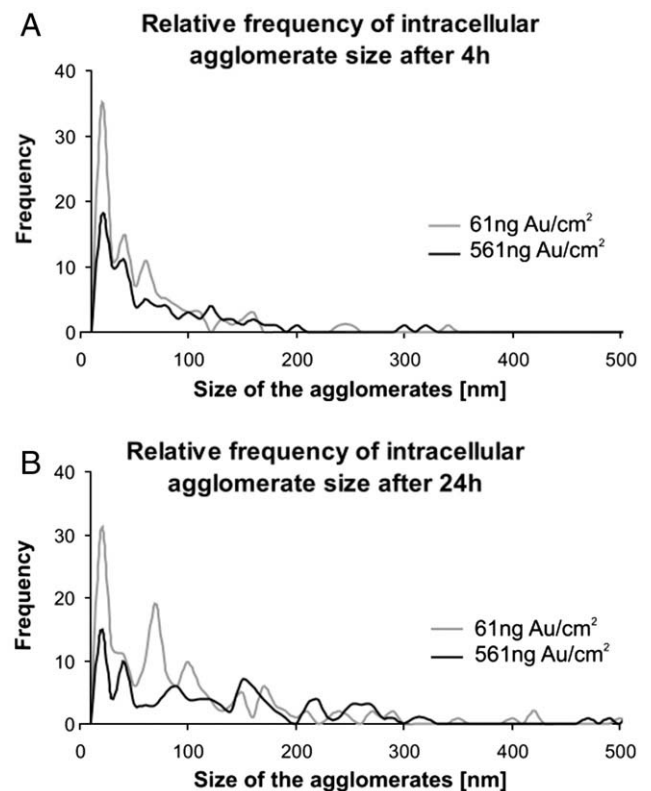


Fig. 5. Relative frequency of the mean agglomerate diameter after 4 h (A) and 24 h (B) incubation times as determined by TEM analysis. At both incubation time points, there are relatively more single particles present at the low exposure concentration compared to the high exposure concentration. However, when comparing the two time points (A vs. B), a shift towards larger agglomerates of more than 100 nm in diameter becomes visible for both exposure concentrations.

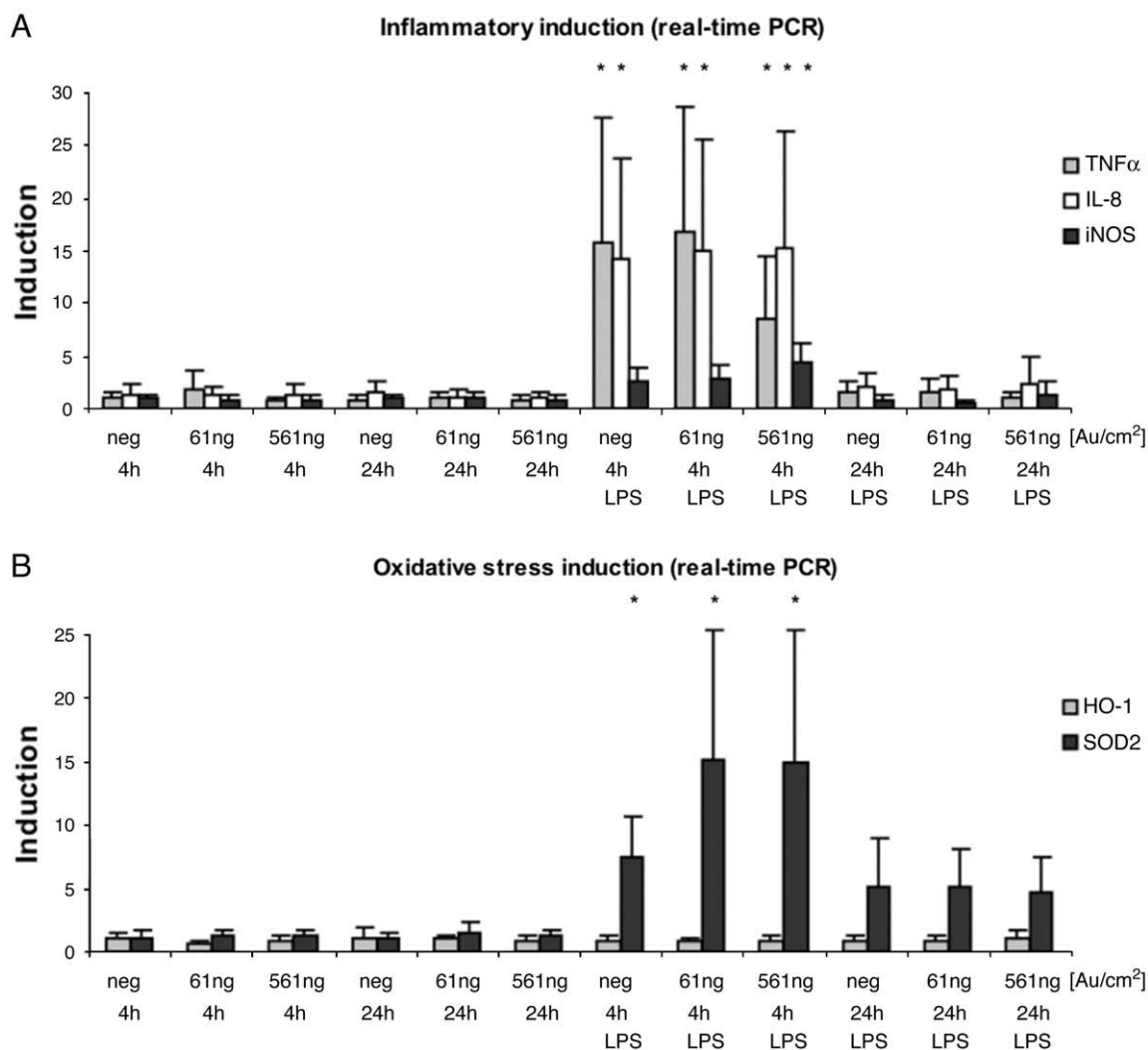


Fig. 6. Gene expression (fold-induction) of inflammatory markers (A) and oxidative stress markers (B) quantified by means of real-time PCR. All results are expressed relative to the negative controls (neg) at 4 h and 24 h. There is no significant increase of pro-inflammatory and oxidative stress markers. LPS leads to a significant induction ($*p < 0.05$) of mRNA after 4 h incubation time, which has vanished after 24 h. No significant synergistic or suppressive effects of particles were observed at any time point.

CSF, TNF α , INF γ were analyzed after 24 h incubation time with a multiplex ELISA method (Fig. 7).

Inflammatory markers showed a significant induction of mRNA due to LPS at 4 h incubation time (Fig. 6A). This increase was no longer observable after 24 h incubation. No significant effect due to particle exposure was revealed, and also not in an inflammatory stimulated environment (pre-stimulation with LPS). The oxidative stress marker SOD2 was also significantly induced by LPS at 4 h, but HO-1 did not react upon LPS exposure (Fig. 6B). No adverse particle effects were measured at any time point and concentration and no synergistic effects could be observed in combination with LPS stimulation. The same findings were observed for inflammatory cytokine release measured by ELISA (Fig. 7).

Discussion

In this study the uptake and possible adverse effects of 15 nm gold particles were analyzed in a triple cell co-culture model exposed at the air–liquid interface. The particles were found to enter the cells in a concentration dependent way and were translocated through the epithelium to dendritic cells located at the basal side. No significant induction of oxidative stress or inflammatory response due to the gold NPs was observed, neither any synergistic or suppressive effect in an inflammatory stimulated system.

The two gold concentrations applied via the nebulizer in these experiments resulted in a deposition of 61 ng/cm² and 561 ng/cm² on the cells. A further increase in the exposure concentration was limited, since multiple exposures would increase the liquid layer (14 μ m for 1 mL of colloidal gold) and hence mitigate or abolish the air–liquid interface effect. Compared to submerged exposure conditions these concentrations might seem to be low. However, it has to be considered, that the dynamics of gold NPs with a diameter ≤ 40 nm in suspensions is driven by diffusion and not by sedimentation (according to equations published by Limbach et al. (2005) which drastically reduces the number of particles deposited on the cells under submerged conditions. It is therefore considered that the exposure concentrations used in the current experiments are in a comparable range with other studies and any absent cellular response can not be related to a too low NP exposure concentration. Table 2 shows a comparison between different gold NP concentrations and their effects, used in different published experiments. Furthermore, the dispersal of mainly single particles onto the cells was confirmed: the measurement of the particle size distribution prior to exposure showed only low agglomeration in the suspension (Fig. 1A) which was also qualitatively observed after particle deposition on TEM grids (Fig. 1B).

In order to evaluate the total particle uptake and the translocation rate towards the basal side where the dendritic cells were localized,

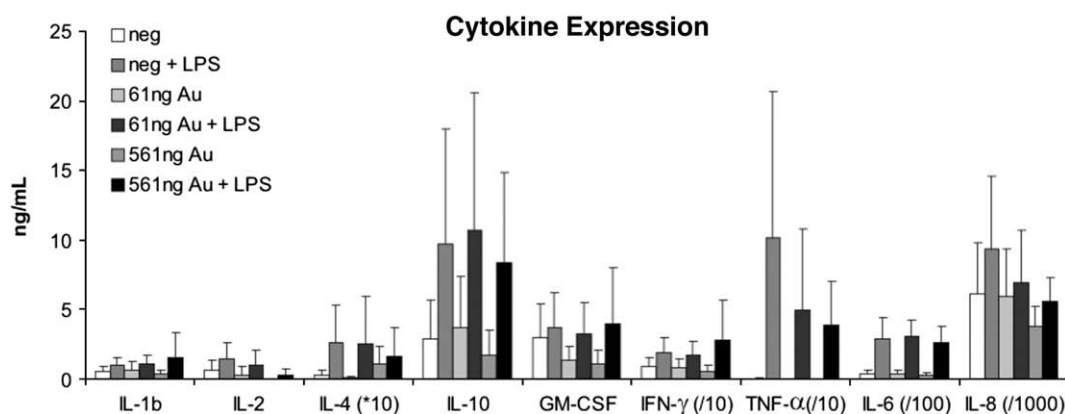


Fig. 7. Protein expression of pro- and anti-inflammatory cytokines. No significant effect on inflammatory cytokine release can be approved due to the exposure to gold NPs. The pre-stimulation with LPS causes a distinct increase in pro- and anti-inflammatory cytokine levels. However, standard deviations of the experiments are too high to assure a significant induction. Synergistic or suppressive effects of gold NPs with LPS could not be found.

the uptake of particles was estimated per mm² cell layer of the upper and the basal side of the triple cell co-culture. The results show a 60% particle uptake rate for the lower exposure concentration but only a 20% uptake rate for the higher exposure concentrations, which might be due to a concentration dependent saturation in particle internalization. Between 4 h and 24 h there was only a marginal increase in intracellular particle numbers for both exposure concentrations, inferring that either most particle uptake occurred during the first four hours or an established equilibrium between endo- and exocytosis. The translocation through the transwell membrane could be confirmed and particles could be identified in dendritic cells (Fig. 4B). It is postulated that particles are either sampled by macrophages and delivered to dendritic cells, or that the dendritic cells themselves extend processes between epithelial cells through the tight junctions to collect the particles (Blank et al., 2007). While the translocation rate remained equal at 4 h and 24 h after exposure to the higher concentration, almost no particles could be detected at the basal side 4 h after exposure to the lower concentration. This effect had vanished after 24 h, which probably means that the translocation process at lower particle dose was slower. A further increase in agglomerate size with time was observed (Fig. 5), which may be explained by particle agglomeration within the cells with time. Since particles were observed in vesicles, it is very likely that this effect occurs due to intracellular vesicle trafficking and fusion after particle uptake.

An evaluation of quantitative particle localization within the different cells could not be performed, since conventional TEM does not allow an exact differentiation of the cell types. The comparison of the average cell number per mm² and the number of intracellular particles per mm² shows that approximately 2400 and 7000 particles per cell were found after exposure to low and high NP concentration, respectively. The correlative particle distribution between the three cell types was previously described with fluorescent polystyrene NPs (Rothen-Rutishauser et al., 2007), showing a preferential uptake by MDM and MDCC.

In the present study, the potential cytotoxic effect of gold particles was investigated by measuring gene expression of inflammatory cytokines and oxidative stress markers at 4 h and 24 h and protein induction of pro- and anti-inflammatory cytokines at 24 h. These two time points were chosen after pre-experimental studies with different incubation times. Effects due to the exposure method have been excluded in previous studies (Schmid et al., 2009) and a internal negative control with cells which were not exposed in the ALICE, were added to the study for each experiment, to factor out side effects (data not shown). The results clearly showed, that no oxidative or inflammatory effects due to particle exposure could be observed in

Table 2

Published results on size, concentration and effects *in vitro* for gold NPs in suspension.

Particle size	μM Au	Effects (cell line)	Reference
1.4 nm	0.2–2.5*	Reduced cell viability after 24 h, with IC ₅₀ values dependent on cell lines (0.3–2.3 μM) (various cell lines e.g. HeLa, Hek-12, MV3)	(Tsoli et al., 2005)
0.8, 1.2, 1.4, 1.8, 15 nm	10–6300*	Particles below 2 nm are cytotoxic and cause apoptosis within 12 h; 1.4 nm particles show the lowest IC ₅₀ value (40–60 μM) (cell lines: HeLa, L929 fibroblasts, SK-Mel-28, JJ4A1)	(Pan et al., 2007)
2 nm positive and negative charged	0.4–7.4*	Vesicle leakage and reduced cell viability after 1 h in positively charged particles only (LC ₅₀ : 1 μM) (COS-1 cell line)	(Goodman et al., 2004)
4 nm	10–100*	No reduction in cell viability after 72 h or pro-inflammatory cytokine release at 24 h (RAW264.7 murine macrophage-like cells)	(Shukla et al., 2005)
13 nm	500–4000 (100–800* μg/mL Au)	Apoptosis and morphological deformation at 2 days–6 days (CF-31 human dermal fibroblast cells)	(Pernodet et al., 2006)
13 nm	10–80*	Nitric oxygen release in fresh plasma serum after 5 min (fresh human plasma serum)	(Jia et al., 2009)
18 nm with coatings	0.1–250*	No reduction in cell viability after 72 h (K562 human leukemia cell)	(Connor et al., 2005)
18 nm	48–480*	No changes in gene expression after 6 h (HeLa cervical cancer cells)	(Khan et al., 2007)
15 nm ALICE	200–2000 (0.3–2.3 μg/6-well)	No induction of oxidative stress markers and inflammatory cytokines (human triple cell co-culture including primary cells)	Current study

Except for the study by Jia et al. (2009) all studies were completed with cell culture lines. The gold particle concentration values given in the publications are indicated *, other values were approximately calculated by the molar mass of gold. Values of 50% lethality (LC₅₀) and 50% inhibition (IC₅₀) and were given in some studies.

this experimental setup for all time points and all gold exposure concentrations. Inflammatory pre-stimulation with LPS resulted in an mRNA induction of marker genes which are known to be regulated by inflammatory stimuli. The oxidative stress marker SOD2 also showed an up regulation after LPS stimulation whereas HO-1 did not, although diverse studies have shown an increase of HO-1 after LPS stimulation in macrophages (Srisook and Cha, 2004) as well as in lung tissue (Zhan et al., 2006). We assume that the observed oxidative stress response of SOD2 was mainly triggered by the response of epithelial cells toward TNF α (Xu et al., 1999), which is not involved in the induction pathway of HO-1 (up to 25 $\mu\text{g}/\text{mL}$) (Wijayanti et al., 2004). LPS primarily acts on macrophages and dendritic cells potentially initiating a HO-1 induction, however we assume that the reaction was under the detection limit in our triple cell co-culture system with a low ratio of MDM, MDCC towards ECs. The primers have been tested previously and HO-1 induction could be measured after air-liquid interface exposure of A549 cells on ZnO particles (personal communication with A.-G. Lenz), and therefore methodological artefacts are excluded.

Cytokine release after 24 h post-exposure showed similar results as mRNA induction at 4 h. All cytokines were expressed in an increased amount after LPS stimulation, but neither the particles themselves nor any synergistic or suppressive effects could be observed.

Since the experiments were performed with primary cultures of MDM and MDCC, it is not surprising that the experiments showed quite a high standard deviation, although experiments were repeated six times. A correlation between the number of MDM and MDCC per transwell and the immune response due to LPS could be excluded by comparing high response and low response experiments with their respective number of MDM and MDCC in the triple cell co-culture system.

It can be summarized that although the gold particles enter the cells of the triple cell co-culture model, no adverse effects could be observed, not even in an inflammation stimulating environment. Comparing the current results with those from other studies (summarized in Table 2), we conclude, that non functionalized gold particles with a size of 13–20 nm in diameter do not cause acute adverse effects. However, toxic effects have been shown for smaller particles with a diameter of 2 nm or less (Pan et al., 2007; Tsoli et al., 2005). This size effect could be explained by an increased catalytic activity for particles with less than 3–5 nm as described by Hvolbaek et al. (2007) or by potential interaction with the DNA for particles equal or smaller than 1.4 nm (Liu et al., 2003). A short term effect of NO release with 13 nm particles as observed by Jia et al. (2009), could not be detected in the triple cell co-culture system after 4 h of incubation when measuring mRNA expression of iNOS. The question remains as to whether morphological changes would also occur after 6 days of incubation at similar exposure concentrations as described by Pernodet et al. (2006). It is not possible to answer this question with our triple cell co-culture system since it can not be maintained for more than 48 h. Therefore, long term *in vivo* studies are needed to entirely exclude adverse effects of gold NPs before applying them in nanomedicine.

Acknowledgments

The authors would like to thank Mr. Bukalis and Mrs. Alber for performing the neutron-activated gamma spectroscopic determination of the mass of the gold nanoparticles, Alexander Wenk, Helga Hinze-Heyn, Barbara Krieger, Andrea Stokes and Mohamed Ouanella for their excellent technical assistance and Kirsten Dobson for proof reading the manuscript.

This study was supported by grants of the AnimalFreeResearch Foundation, the Doerenkamp-Zbinden-Foundation, the Deutsche

Forschungs Gemeinschaft (DFG), Swiss National Science Foundation (3100A0_118420) and the Helmholtz Association.

References

- Baddeley, A.J., Gundersen, H.J.G., Cruz-Orive, L.M., 1986. Estimation of surface-area from vertical sections. *J. Microsc.* 142, 259–276.
- Blank, F., Rothen-Rutishauser, B., Gehr, P., 2007. Dendritic cells and macrophages form a transepithelial network against foreign particulate antigens. *Am. J. Respir. Cell Mol. Biol.* 36, 669–677.
- Brandenberger, C., Rothen-Rutishauser, B., Blank, F., Gehr, P., Muhlfeld, C., 2009. Particles induce apical plasma membrane enlargement in epithelial lung cell line depending on particle surface area dose. *Respir. Res.* 10, 22.
- Chan, R.C.F., Wang, M.Y., Li, N., Yanagawa, Y., Onoe, K., Lee, J.J., Nel, A.E., 2006. Pro-oxidative diesel exhaust particle chemicals inhibit LPS-induced dendritic cell responses involved in T-helper differentiation. *J. Allergy Clin. Immunol.* 118, 455–465.
- Chen, Y.H., Tsai, C.Y., Huang, P.Y., Chang, M.Y., Cheng, P.C., Chou, C.H., Chen, D.H., Wang, C.R., Shiau, A.L., Wu, C.L., 2007. Methotrexate conjugated to gold nanoparticles inhibits tumor growth in a syngeneic lung tumor model. *Mol. Pharm.* 4, 713–722.
- Cho, W.S., Cho, M., Jeong, J., Choi, M., Cho, H.Y., Han, B.S., Kim, S.H., Kim, H.O., Lim, Y.T., Chung, B.H., Jeong, J., 2009. Acute toxicity and pharmacokinetics of 13 nm-sized PEG-coated gold nanoparticles. *Toxicol. Appl. Pharmacol.* 236, 16–24.
- Connor, E.E., Mwamuka, J., Gole, A., Murphy, C.J., Wyatt, M.D., 2005. Gold nanoparticles are taken up by human cells but do not cause acute cytotoxicity. *Small* 1, 325–327.
- de Haar, C., Hassing, I., Bol, M., Bleumink, R., Pieters, R., 2006. Ultrafine but not fine particulate matter causes airway inflammation and allergic airway sensitization to co-administered antigen in mice. *Clin. Exp. Allergy* 36, 1469–1479.
- Dhar, S., Reddy, E.M., Shiras, A., Pokharkar, V., Prasad, B.L., 2008. Natural gum reduced/stabilized gold nanoparticles for drug delivery formulations. *Chemistry* 14, 10244–10250.
- Goodman, C.M., McCusker, C.D., Yilmaz, T., Rotello, V.M., 2004. Toxicity of gold nanoparticles functionalized with cationic and anionic side chains. *Bioconjug. Chem.* 15, 897–900.
- Griffiths, G., 1993. *Fine Structure Immunocytochemistry*. Springer-Verlag, Berlin Heidelberg.
- Herzog, E., Byrne, H.J., Casey, A., Davoren, M., Lenz, A.G., Maier, K.L., Duschl, A., Oostingh, G.J., 2009a. SWCNT suppress inflammatory mediator responses in human lung epithelium *in vitro*. *Toxicol. Appl. Pharmacol.* 234, 378–390.
- Herzog, E., Byrne, H.J., Davoren, M., Casey, A., Duschl, A., Oostingh, G.J., 2009b. Dispersion medium modulates oxidative stress response of human lung epithelial cells upon exposure to carbon nanomaterial samples. *Toxicol. Appl. Pharmacol.* 236, 276–281.
- Hofer, T.P., Bitterle, E., Beck-Speier, I., Maier, K.L., Frankenberger, M., Heyder, J., Ziegler-Heitbrock, L., 2004. Diesel exhaust particles increase LPS-stimulated COX-2 expression and PGE2 production in human monocytes. *J. Leukoc. Biol.* 75, 856–864.
- Holt, P.G., Schon-Hegrad, M.A., McMenamin, P.G., 1990. Dendritic cells in the respiratory tract. *Int. Rev. Immunol.* 6, 139–149.
- Hussain, S.M., Hess, K.L., Gearhart, J.M., Geiss, K.T., Schlager, J.J., 2005. In vitro toxicity of nanoparticles in BRL 3A rat liver cells. *Toxicol. In Vitro* 19, 975–983.
- Hvolbaek, B., Janssens, T.V.W., Clausen, B.S., Falsig, H., Christensen, C.H., Nørskov, J.K., 2007. Catalytic activity of Au nanoparticles. *Nano Today* 2, 14–18.
- Jain, P.K., Huang, X., El-Sayed, I.H., El-Sayed, M.A., 2008. Noble metals on the nanoscale: optical and photothermal properties and some applications in imaging, sensing, biology, and medicine. *Acc. Chem. Res.* 41, 1578–1586.
- Jia, H.Y., Liu, Y., Zhang, X.J., Han, L., Du, L.B., Tian, Q., Xu, Y.C., 2009. Potential oxidative stress of gold nanoparticles by induced-NO releasing in serum. *J. Am. Chem. Soc.* 131, 40–41.
- Joshi, H.M., Bhumkar, D.R., Joshi, K., Pokharkar, V., Sastry, M., 2006. Gold nanoparticles as carriers for efficient transmucosal insulin delivery. *Langmuir* 22, 300–305.
- Khaing Oo, M.K., Yang, X., Du, H., Wang, H., 2008. 5-aminolevulinic acid-conjugated gold nanoparticles for photodynamic therapy of cancer. *Nanomedicine* 3, 777–786.
- Khan, J.A., Pillai, B., Das, T.K., Singh, Y., Maiti, S., 2007. Molecular effects of uptake of gold nanoparticles in HeLa cells. *Chembiochemical* 8, 1237–1240.
- Kreyling, W.G., Semmler-Behnke, M., Moller, W., 2006. Ultrafine particle-lung interactions: does size matter? *J. Aerosol Med.* 19, 74–83.
- Kwon, Y.M., Xia, Z., Glyn-Jones, S., Beard, D., Gill, H.S., Murray, D.W., 2009. Dose-dependent cytotoxicity of clinically relevant cobalt nanoparticles and ions on macrophages *in vitro*. *Biomed. Mater.* 4.
- Li, J.L., Wang, L., Liu, X.Y., Zhang, Z.P., Guo, H.C., Liu, W.M., Tang, S.H., 2009. In vitro cancer cell imaging and therapy using transferrin-conjugated gold nanoparticles. *Cancer Lett.* 274, 319–326.
- Lieber, M., Smith, B., Szakal, A., Nelsonreese, W., Todaro, G., 1976. Continuous tumor-cell line from a human lung carcinoma with properties of type-II alveolar epithelial cells. *Int. J. Cancer* 17, 62–70.
- Limbach, L.K., Li, Y., Grass, R.N., Brunner, T.J., Hintermann, M.A., Muller, M., Gunther, D., Stark, W.J., 2005. Oxide nanoparticle uptake in human lung fibroblasts: effects of particle size, agglomeration, and diffusion at low concentrations. *Environ. Sci. Technol.* 39, 9370–9376.
- Liu, Y., Meyer-Zaika, W., Franzka, S., Schmid, G., Tsoli, M., Kuhn, H., 2003. Gold-cluster degradation by the transition of B-DNA into A-DNA and the formation of nanowires. *Angew. Chem., Int. Ed. Engl.* 42, 2853–2857.

- Mayhew, T.M., 2008. Taking tissue samples from the placenta: an illustration of principles and strategies. *Placenta* 29, 1–14.
- Mühlfeld, C., Rothen-Rutishauser, B., Vanhecke, D., Blank, F., Gehr, P., Ochs, M., 2007. Visualization and quantitative analysis of nanoparticles in the respiratory tract by transmission electron microscopy. *Part Fibre Toxicol.* 4, 11.
- Nel, A., Xia, T., Madler, L., Li, N., 2006. Toxic potential of materials at the nanolevel. *Science* 311, 622–627.
- Oberdörster, G., Oberdörster, E., Oberdörster, J., 2005. Nanotoxicology: An emerging discipline evolving from studies of ultrafine particles. *Environ. Health Perspect.* 113, 823–839.
- Olofsson, L., Rindzevicius, T., Pfeiffer, I., Kall, M., Hook, F., 2003. Surface-based gold-nanoparticle sensor for specific and quantitative DNA hybridization detection. *Langmuir* 19, 10414–10419.
- Pan, Y., Neuss, S., Leifert, A., Fischler, M., Wen, F., Simon, U., Schmid, G., Brandau, W., Jahnen-Dechent, W., 2007. Size-dependent cytotoxicity of gold nanoparticles. *Small* 3, 1941–1949.
- Pernodet, N., Fang, X., Sun, Y., Bakhtina, A., Ramakrishnan, A., Sokolov, J., Ulman, A., Rafailovich, M., 2006. Adverse effects of citrate/gold nanoparticles on human dermal fibroblasts. *Small* 2, 766–773.
- Rosi, N.L., Giljohann, D.A., Thaxton, C.S., Lytton-Jean, A.K.R., Han, M.S., Mirkin, C.A., 2006. Oligonucleotide-modified gold nanoparticles for intracellular gene regulation. *Science* 312, 1027–1030.
- Rothen-Rutishauser, B.M., Kiama, S.G., Gehr, P., 2005. A three-dimensional cellular model of the human respiratory tract to study the interaction with particles. *Am. J. Respir. Cell Mol. Biol.* 32, 281–289.
- Rothen-Rutishauser, B., Muhlfield, C., Blank, F., Musso, C., Gehr, P., 2007. Translocation of particles and inflammatory responses after exposure to fine particles and nanoparticles in an epithelial airway model. *Part Fibre Toxicol.* 4, 9.
- Sallusto, F., Cella, M., Danieli, C., Lanzavecchia, A., 1995. Dendritic cells use macropinocytosis and the mannose receptor to concentrate macromolecules in the major histocompatibility complex class-II compartment—down-regulation by cytokines and bacterial products. *J. Exp. Med.* 182, 389–400.
- Schmid, O., Ferron, G.A., Lentner, B., Lenz, A.G., Brandenberger, C., Rothen-Rutishauser, B., Gehr, P., Kreyling, W., Schulz, H., Karg, E., 2009. Development of a quantitative and easy-to-use system for thin-film deposition of nanoparticle suspensions onto cells at the air-liquid interface (ALI). *J. Aerosol Med. Pulm. Drug Deliv.* 22, 199 (Conference Abstract).
- Selvakannan, P.R., Mandal, S., Phadtare, S., Gole, A., Pasricha, R., Adyanthaya, S.D., Sastry, M., 2004. Water-dispersible tryptophan-protected gold nanoparticles prepared by the spontaneous reduction of aqueous chloroaurate ions by the amino acid. *J. Colloid Interface Sci.* 269, 97–102.
- Shukla, R., Bansal, V., Chaudhary, M., Basu, A., Bhonde, R.R., Sastry, M., 2005. Biocompatibility of gold nanoparticles and their endocytotic fate inside the cellular compartment: A microscopic overview. *Langmuir* 21, 10644–10654.
- Srisook, K., Cha, Y.N., 2004. Biphasic induction of heme oxygenase-1 expression in macrophages stimulated with lipopolysaccharide. *Biochem. Pharmacol.* 68, 1709–1720.
- Small, J.V., 1968. Measurement of section thickness. Fourth Eur. Conf. Electron Microsc. 609–610.
- Stoeger, T., Reinhard, C., Takenaka, S., Schroeppel, A., Karg, E., Ritter, B., Heyder, J., Schulz, H., 2006. Instillation of six different ultrafine carbon particles indicates a surface area threshold dose for acute lung inflammation in mice. *Environ. Health Perspect.* 114, 328–333.
- Teeguarden, J.G., Hinderliter, P.M., Orr, G., Thrall, B.D., Pounds, J.G., 2007. Particokinetics in vitro: dosimetry considerations for in vitro nanoparticle toxicity assessments. *Toxicol. Sci.* 95, 300–312.
- Tsoli, M., Kuhn, H., Brandau, W., Esche, H., Schmid, G., 2005. Cellular uptake and toxicity of Au55 clusters. *Small* 1, 841–844.
- Wangoo, N., Bhasin, K.K., Mehta, S.K., Suri, C.R., 2008. Synthesis and capping of water-dispersed gold nanoparticles by an amino acid: bioconjugation and binding studies. *J. Colloid Interface Sci.* 323, 247–254.
- Weibel, E.R., Hsia, C.C., Ochs, M., 2007. How much is there really? Why stereology is essential in lung morphometry. *J. Appl. Physiol.* 102, 459–467.
- Wijayanti, N., Huber, S., Samoylenko, A., Kietzmann, T., Immenschuh, S., 2004. Role of NF- κ B and p38 MAP kinase signaling pathways in the lipopolysaccharide-dependent activation of heme oxygenase-1 gene expression. *Antioxid. Redox Signal.* 6, 802–810.
- Xu, Y., Kinningham, K.K., Devalaraja, M.N., Yeh, C.C., Majima, H., Kasarskis, E.J., St Clair, D.K., 1999. An intronic NF- κ B element is essential for induction of the human manganese superoxide dismutase gene by tumor necrosis factor- α and interleukin-1 β . *DNA Cell Biol.* 18, 709–722.
- Zhan, L.Y., Xia, Z.Y., Chen, C., Wang, X.Y., 2006. Effect of radix paeoniae rubra on the expression of HO-1 and iNOS in rats with endotoxin-induced acute lung injury. 9, 181–186.